Journal of Power Sources 183 (2008) 34–42

Contents lists available at ScienceDirect

Journal of Power Sources

journal homepage: www.elsevier.com/locate/jpowsour

Development of high performance carbon composite catalyst for oxygen reduction reaction in PEM Proton Exchange Membrane fuel cells

Vijayadurga Nallathambi, Jong-Won Lee, Swaminatha P. Kumaraguru, Gang Wu, Branko N. Popov*

Center for Electrochemical Engineering, Department of Chemical Engineering, University of South Carolina, Columbia, SC 29208, USA

ARTICLE INFO

Article history:
Received 7 March 2008
Received in revised form 28 April 2008
Accepted 1 May 2008
Available online 15 May 2008

Keywords:
Carbon composite catalyst
Nitrogen functional group
Oxygen reduction
Polymer electrolyte membrane fuel cell
Transition metal

ABSTRACT

Highly active and stable carbon composite catalysts for oxygen reduction in PEM fuel cells were developed through the high-temperature pyrolysis of Co–Fe–N chelate complex, followed by the chemical post-treatment. A metal-free carbon catalyst was used as the support. The carbon composite catalyst showed an onset potential for oxygen reduction as high as 0.87 V (NHE) in H_2SO_4 solution, and generated less than 1% H_2O_2. The PEM fuel cell exhibited a current density as high as 0.27 A cm^{-2} at 0.6 V and 2.3 A cm^{-2} at 0.2 V for a catalyst loading of 6.0 mg cm^{-2}. No significant performance degradation was observed over 480 h of continuous fuel cell operation with 2 mg cm^{-2} catalyst under a load of 200 mA cm^{-2} as evidenced by a resulting cell voltage of 0.32 V with a voltage decay rate of 80 μV h^{-1}. Materials characterization studies indicated that the metal–nitrogen chelate complexes decompose at high pyrolysis temperatures above 800 °C, resulting in the formation of the metallic species. During the pyrolysis, the transition metals facilitate the incorporation of pyridinic and graphitic nitrogen groups into the carbon matrix, and the carbon surface doped with nitrogen groups is catalytically active for oxygen reduction.

1. Introduction

Platinum is considered the best electrocatalyst for the four-electron reduction of oxygen to water in acidic environments as it provides the lowest overpotentials and the highest stability [1–5]. However, even on pure Pt, potentials in excess of 300 mV are lost from the thermodynamic potential for oxygen reduction due to competing water activation and sluggish kinetics. Furthermore, oxygen undergoes non-dissociative adsorption on Pt metals accompanied by some dissociative adsorption, which results in Pt oxidation. Most importantly, Pt remains an expensive metal of low abundance.

Since Jasinski's discovery of the catalytic properties of cobalt phthalocyanines [6], there has been a considerable research on non-precious metal catalysts such as: (i) porphyrin-based macrocyclic compounds of transition metals (e.g., cobalt phthalocyanines and iron tetramethoxyphenyl porphyrin (Fe-TMPP)) [7–23], (ii) vacuum-deposited cobalt and iron compounds (e.g., Co–C–N and Fe–C–N) [24,25], and (iii) metal carbides, nitrides and oxides (e.g., FeC_x, TaO_xN_y, MnO_x/C) [26,27]. Pyrolysis at higher temperatures than 800 °C in an inert or NH_3 atmosphere led to the improvement in activity and stability of the catalysts to some extent, but none of the above catalysts are active or stable enough to be used as oxygen reduction catalysts for PEM fuel cells. Due to low selectivity (H_2O_2 amount >5%) and poor stability, the transition metal-based catalysts reported in the literature so far do not qualify as catalyst for oxygen reduction.

There is disagreement in the literature regarding the catalytic reaction site for oxygen reduction and the relevant mechanism on non-precious metal catalysts. The most commonly accepted hypothesis is that the metal–N_4 center bound to the carbon support is catalytically active, and the central metal ion in the macrocycle plays a crucial role in the oxygen reduction reaction [7–23,28]. Beck [28] has proposed that oxygen reduction on N_4-chelates of transition metal occurs via a modified "redox catalysis" mechanism. That is, an oxygen molecule is adsorbed on the catalyst metal center to form an oxygen–catalyst adduct, followed by electron transfer from the metal center and the regeneration of the reduced N_4-chelates. From the analysis of Fe-based catalysts by time-of-flight secondary ion mass spectrometry, Dodelet and co-workers [14] have maintained that two different catalytic sites, i.e., FeN_4/C and FeN_2/C, coexist in the catalysts, irrespective of the Fe precursors used. Here, FeN_4/C represents an Fe ion coordinated to four nitrogen atoms of the pyrrolic type, and FeN_2/C stands for an Fe ion coordinated to two nitrogen atoms of the pyridinic type.

On the other hand, Yeager [29] found that after the heat-treatment of Co-TMPP and Fe-TMPP at 800 °C, neither Co nor Fe was detected in the Mössbauer spectra in a form corresponding to

* Corresponding author. Tel.: +1 803 777 7314; fax: +1 803 777 8265.
E-mail address: popov@engr.sc.edu (B.N. Popov).

0378-7753/$ – see front matter © 2008 Elsevier B.V. All rights reserved.
doi:10.1016/j.jpowsour.2008.05.020

coordination with nitrogen. Yeager and Wiesener [30] have suggested that the transition metals do not act as an active reaction site for oxygen reduction, but rather serve primarily to facilitate the stable incorporation of nitrogen into the graphitic carbon during high-temperature pyrolysis of metal–nitrogen complexes. This means that high-temperature pyrolysis in the presence of transition metals yields a carbonaceous layer with a large amount of nitrogen groups that are catalytically active for oxygen reduction.

Nitrogen-containing carbons have been typically prepared using implantation through NH_3 or HCN treatment of carbon at high temperatures. The experimental measurements of nitrided Ketjen black indicated an onset potential for oxygen reduction of approximately 0.5 V (NHE) compared to that of 0.2 V (NHE) for un-treated carbon [31,32]. Another way to prepare carbons with a controlled nitrogen content is to synthesize carbon powder using nitrogen-containing polymer precursors, followed by a physical or chemical activation process [33–38]. Matter et al. [39–41] prepared an active non-metal catalyst for oxygen reduction through decomposition of acetonitrile vapor over an alumina support containing 2 wt% Fe or Ni. The results obtained for oxygen electroreduction by using a rotating ring-disk electrode (RRDE) technique indicated only 100 mV greater overpotential than Pt catalyst, but the measured currents were in μA range. The catalyst activity was attributed to pyridinic nitrogen incorporated into edge planes as determined by X-ray photoelectron spectroscopy (XPS). However, a measurable cathode current was observed in the RRDE experiments only at the potential range for H_2O_2 formation (i.e., below approximately 0.6 V (NHE)).

At the University of South Carolina, recently, we have developed a carbon-based metal-free catalyst with improved activity and selectivity using organic nitrogen precursors [42–44]. The metal-free catalyst was synthesized through surface modification of porous carbon blacks with different functional groups such as oxygen and nitrogen, followed by various thermal and chemical activation processes. Introduction of surface functional groups decreased the activation overpotential by 500 mV and the H_2O_2 amount to almost zero, in comparison to the as-received carbon black.

The objective of the present study is to develop a highly active and stable carbon composite catalyst for oxygen reduction in PEM fuel cells. The carbon composite catalyst was synthesized using the metal-free carbon catalyst as a support through the three consecutive steps: (i) the deposition of Co–N or Co–Fe–N chelate complex, and (ii) the high-temperature pyrolysis, and (iii) the chemical post-treatment. Metal additives such as Co and Fe were used as an agent to facilitate and stabilize the incorporation of nitrogen within the carbon matrix. The RRDE technique was performed to determine the catalytic activity and selectivity to four-electron oxygen reduction. The catalyst performance was also evaluated in a single PEM fuel cell. The synthesized catalysts were characterized using a wide range of analytical techniques in an attempt to identify the active reaction sites for oxygen reduction.

2. Experimental

2.1. Synthesis of carbon composite catalysts

A carbon-based metal-free catalyst was prepared by activating a porous carbon black with surface functional groups such as oxygen and nitrogen as described elsewhere [42–44]. Briefly, the as-received carbon black (e.g., Vulcan XC 72, Ketjen black EC 300J, Black Pearl 2000, etc.) was treated in a concentrated HCl solution to remove metal impurities present on the carbon. Next, the HCl-treated carbon was refluxed in a concentrated HNO_3 solution at 80 °C, in order to introduce oxygen functional groups into the carbon surface. Finally, the oxidized carbon surface was modified with nitrogen functional groups by reacting the carbon with nitrogen-containing organic precursors and thermal/chemical activation processes.

The carbon composite catalyst was synthesized using the metal-free carbon support through the three consecutive steps: (i) the deposition of Co–N or Co–Fe–N chelate complex on the support, and (ii) the high-temperature pyrolysis, and (iii) the chemical post-treatment (acid leaching). $Co(NO_3)_2$, $FeSO_4$, and ethylene diamine ($H_2NCH_2CH_2NH_2$) were used as Co-, Fe- and N-precursors, respectively. Desired amounts of $Co(NO_3)_2$ and/or $FeSO_4$ were dissolved in ethanol. A mixture of ethylene diamine and ethanol was added drop-wise into the reaction mixture, followed by vigorous stirring for 1 h. In the reaction mixture, the atomic ratio of metal:nitrogen varied between 1:4 and 1:24. The metal-free carbon support was added into the reaction mixture and refluxed at 85 °C for 4 h. The solvents were removed in a rotary evaporator at 80 °C under vacuum, and the resulting powder specimen was heat-treated (pyrolized) in an argon atmosphere at different temperatures of 600–900 °C for 1 h. In order to remove excess metal elements deposited on the support, the pyrolized sample was treated with 0.5 M H_2SO_4 solution at 90 °C for 4 h, and washed thoroughly with deionized water.

2.2. Rotating ring-disk electrode measurements

The RRDE experiments were performed in a three-electrode electrochemical cell using a bi-potentiostat (Pine Instruments) at room temperature. An RRDE with Pt ring (5.52 mm inner-diameter and 7.16 mm outer-diameter) and glassy carbon disk (5.0 mm diameter) was employed as the working electrode. The catalyst ink was prepared by blending the catalyst powder (8 mg) with isopropyl alcohol (1 mL) in an ultrasonic bath. The catalyst ink (15 μL) was deposited onto the glassy carbon disk that had been polished with Al_2O_3 powder. After drying, 5 μL of a mixture of Nafion™ solution (5 wt%, Alfa Aesar) and isopropyl alcohol was coated onto the catalyst layer to ensure better adhesion of the catalyst on the glassy carbon substrate. The electrolyte was 0.5 M H_2SO_4 solution. A platinum mesh and an $Hg/HgSO_4$ electrode (0.64 V vs. NHE) were used as the counter and reference electrodes, respectively. All potentials in this work were referred to a normal hydrogen electrode (NHE).

In order to estimate the double layer capacitance, the electrolyte was deaerated by bubbling with N_2, and the cyclic voltammogram was recorded at 900 rpm by scanning the disk potential between 0.04 and 1.04 V (NHE) at a rate of 5 mV s^{-1}. Then, the voltammogram was evaluated in the oxygen-saturated electrolyte. The oxygen reduction current was taken as the difference between currents measured in the deaerated and oxygen-saturated electrolytes. Since the Pt ring may be contaminated with impurities in the electrolyte, causing a decrease in activity for H_2O_2 oxidation, it was activated by cycling in H_2SO_4 from about −0.05 to 1.3 V (NHE) at 50 mV s^{-1} for 5 min [16]. Immediately after the activation step, the ring potential was held at 1.2 V (NHE).

2.3. Performance test of membrane-electrode assemblies (MEAs)

The cathode catalyst ink was prepared by ultrasonically blending the catalyst powder with Nafion™ solution (5 wt%) and isopropyl alcohol for 2 h. The catalyst ink was sprayed onto a gas diffusion layer (GDL) (ELAT LT 1400 W, E-TEK) until a desired catalyst loading has been achieved. The weight percentages of catalyst powder and Nafion™ in the dried catalyst layer were 75% and 25%, respectively. A commercially available catalyzed GDL (LT140EW Low Temperature ELAT® GDE Microporous Layer, E-TEK) was used as the anode for all fuel cell tests. The anode catalyst was 30 wt% Pt/C and the Pt loading was 0.5 mg cm^{-2}. A thin layer of Nafion™

(0.4 mg cm^{-2}) was coated on both the anode and cathode surfaces. The Nafion™-coated anode and cathode were hot-pressed to a Nafion™ 112 membrane at 140 °C and at 15 atm for 3 min. The geometric area of the MEA used was 5 cm^2.

The MEA tests were carried out in a single cell with serpentine flow channels. Pure H_2 gas humidified at 77 °C and pure O_2 gas humidified at 75 °C were supplied to the anode and cathode compartments, respectively. The flow rates of H_2 and O_2 were 300 and 600 cm^3 min^{-1}, respectively. Polarization experiments were conducted using a fully automated test station (Fuel Cell Technologies Inc.) at 75 °C either or with no back pressure or with a back pressure of 30 psi (2.0 atm) on both compartments.

2.4. Materials characterizations

Extended X-ray absorption fine structure (EXAFS) spectra were recorded at room temperature at beam line X9B of the National Synchrotron Light Source at Brookhaven National Laboratory. The data were collected in the transmission mode. The background removal and edge-step normalization were performed using the FEFFIT 3.42 program, and the experimental EXAFS data were analyzed by the FEFF 7.0 program.

Transmission electron microscopy (TEM) was carried out using a high-resolution Hitachi H-8000 system. In order to identify the crystal structure of the synthesized catalyst, powder X-ray diffraction (XRD) patterns were recorded with a Rigaku 405S5 using a Cu K_α radiation at a scan rate of 1.2° min^{-1}. Inductively coupled plasma-mass spectroscopy (ICP-MS) was performed with an SCIEX ELAN DRCe ICP-MS system (PerkinElmer) to analyze the bulk composition of the catalyst. For chemical analysis of the catalyst surface, XPS was conducted with an ESCA 210 and MICROLAB 310D spectrometer.

3. Results and discussion

3.1. Electrocatalytic properties of the carbon-based metal-free catalysts used as a support for the carbon composite catalyst

Carbon-based metal-free catalysts were synthesized by modifying the porous carbon black with the surface functional groups such as oxygen and nitrogen. Nitrogen groups were incorporated into the graphitic structure using polymerization of low-cost organic precursors (e.g., melamine-formaldehyde, urea-formaldehyde, and selenourea-formaldehyde) and thermal/chemical activation processes.

Fig. 1 presents polarization curves observed on the rotating disk electrodes for the carbon blacks treated by various methods. The RRDE measurements were performed in 0.5 M H_2SO_4 solution saturated with O_2 using a potential scan rate of 5 mV s^{-1} and a rotation speed of 900 rpm. For comparison, the curve measured on the as-received Ketjen black is also shown in Fig. 1. The as-received carbon (curve "a") does not show any catalytic activity towards oxygen reduction. The carbon oxidized with HNO_3 (curve "b") exhibits higher catalytic activity compared with the as-received carbon. The increased activity is attributed to the oxygen functional groups of quinone/hydroquinone generated on the carbon surface during HNO_3 treatment [32,44].

Remarkable increase in the catalytic activity towards oxygen reduction has been achieved with the introduction of nitrogen groups. The metal-free catalysts synthesized by novel methodologies with organic N-precursors (curves "d" and "e") show improved performance when compared with the conventional NH_3-treated carbon (curve "c"). For example, the metal-free catalyst prepared using selenourea-formaldehyde (curve "e") exhibits an onset

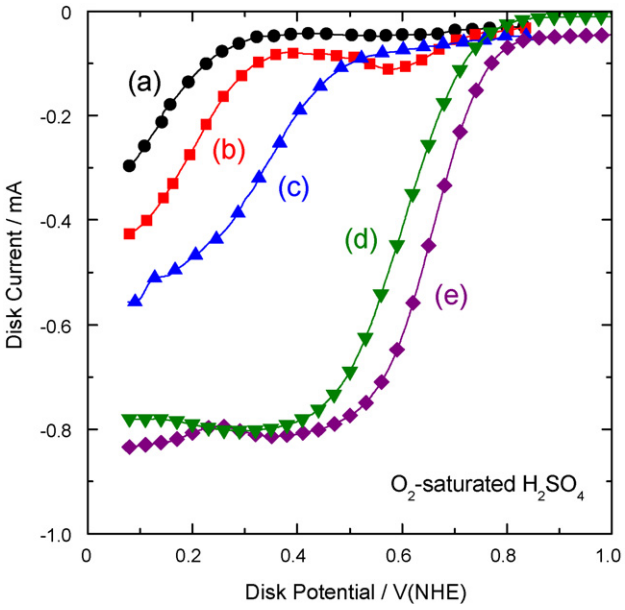

Fig. 1. Polarization curves on the rotating disk electrodes for the carbon (Ketjen) blacks treated by various methods: (a) as-received carbon, (b) HNO_3-treated carbon, (c) NH_3-treated carbon, (d) urea-formaldehyde-modified carbon, and (e) selenourea-formaldehyde-modified carbon. The measurements were performed in 0.5 M H_2SO_4 solution saturated with O_2 using a potential scan rate of 5 mV s^{-1} and a rotation speed of 900 rpm.

potential for oxygen reduction as high as 0.83 V (NHE) and also a well-defined diffusion limiting current which is only observed in Pt-based catalyst.

The oxygen reduction reaction proceeds by two pathways as follows [29]:

$$\begin{array}{ccccc} & & \overset{1}{\overbrace{\qquad\qquad}} & & \\ & & \uparrow \quad\quad \downarrow & & \\ O_{2,b} & \rightarrow & O_{2,a} & \xrightarrow{2} H_2O_{2,a} & \xrightarrow{3} H_2O \\ & & & \downarrow 4 & \\ & & & H_2O_{2,b} & \end{array} \quad (1)$$

where subscripts a and b denote the species adsorbed on the electrode surface and that in the bulk, respectively. O_2 may be directly reduced to H_2O through four-electron transfer (reaction (1)). In parallel, O_2 may be reduced to H_2O_2 via two-electron transfer (reaction (2)), followed by either reduction of H_2O_2 to H_2O (reaction (3)) or transport of the adsorbed H_2O_2 to the bulk solution (reaction (4)). H_2O_2 is believed to be responsible for the deterioration of MEA performance, since the polymer electrolyte membrane and the catalyst degrade over time due to attack by peroxide radicals [12,45]. The amount of H_2O_2 produced was calculated from the RRDE data using Eq. (2) [46]:

$$\%H_2O_2 = \frac{200(I_r/N)}{I_d + (I_r/N)} \quad (2)$$

where I_d, I_r and N mean the disk current, the ring current and the collection efficiency, respectively. Here, the value of N was taken as 0.39.

Table 1 summarizes % H_2O_2 determined at 0.5 V (NHE) for the different metal-free catalysts. It is known that oxygen reduction to H_2O_2 is predominant on most of carboneous materials, since the O—O bond breakage is not feasible. However, the metal-free carbon catalysts, which had been used as a support in this study, generated 0–3% H_2O_2 at 0.5 V (NHE) depending on the precursors used. In this

Table 1
H_2O_2 percentages and number of electrons (n) transferred during oxygen reduction on the metal-free carbon catalysts

Organic precursor used for metal-free catalyst preparation	% H_2O_2	n
Melamine-formaldehyde	28	3.2
Urea-formaldehyde	3	3.6
Selenourea-formaldehyde	0	4.0

The data were obtained at 0.5 V (NHE).

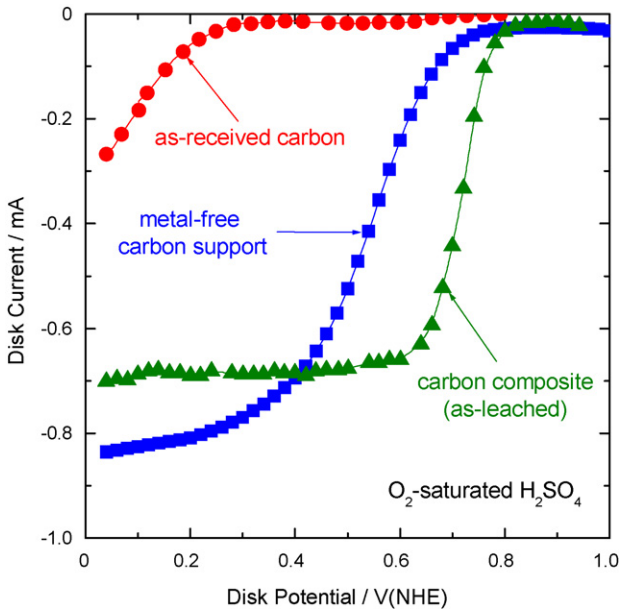

Fig. 2. Polarization curves on the rotating disk electrodes for the as-received carbon, the metal-free carbon support and the carbon composite catalyst (as-leached). The measurements were performed in 0.5 M H_2SO_4 solution saturated with O_2 using a potential scan rate of 5 mV s^{-1} and a rotation speed of 900 rpm.

study, the metal-free carbon modified with urea-formaldehyde was used as a support for preparation of the carbon composite catalyst.

3.2. Electrocatalytic properties of the carbon composite catalyst for oxygen reduction

The carbon composite catalyst was prepared as follows: (i) the $Co_1Fe_1N_x$ deposition on the metal-free carbon support, (ii) the pyrolysis at 900 °C, and (iii) the chemical leaching in 0.5 M H_2SO_4 solution at 90 °C. Fig. 2 shows typical polarization curves on the rotating disk electrodes for the metal-free carbon support and the as-leached carbon composite catalyst. The RRDE measurements were performed in 0.5 M H_2SO_4 using a rotation speed of 900 rpm. For comparison, the curve measured on the as-received carbon is also presented in Fig. 2. The as-received carbon did not show any catalytic activity toward oxygen reduction. The metal-free carbon support exhibited much higher activity when compared

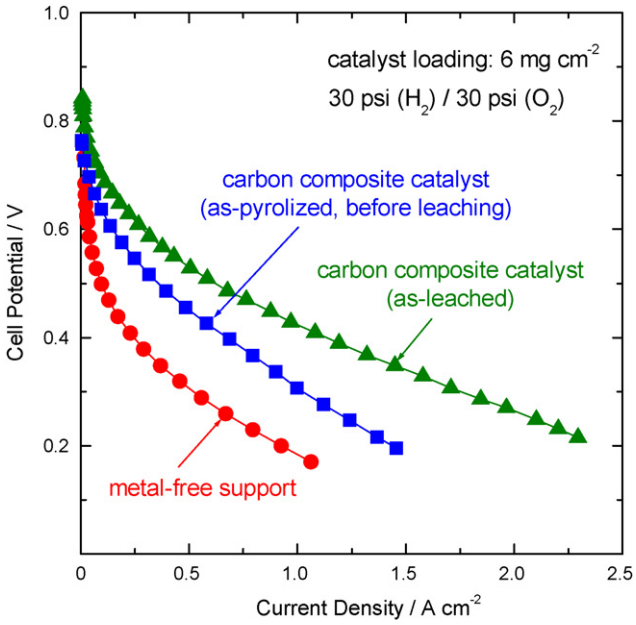

Fig. 3. Polarization curves of PEM fuel cells prepared with the different cathode catalysts: the metal-free carbon support, the as-pyrolized carbon composite catalyst, and the as-leached carbon composite catalyst. The cathode catalyst loadings were maintained at 6.0 mg cm^{-2}. The experiments were performed using 30 psi back pressure on both anode (H_2) and cathode (O_2) compartments.

with the as-received carbon. The increased activity is attributed to the oxygen and nitrogen functional groups introduced on the carbon surface [42–44]. A further improvement in the activity was achieved with the pyrolysis in the presence of $Co_1Fe_1N_x$ complex, followed by the chemical leaching treatment. The carbon composite catalyst showed an onset potential for oxygen reduction as high as 0.87 V (NHE) and also a well-defined diffusion limiting current.

Table 2 summarizes % H_2O_2 as a function of disk potential determined for the different catalysts: (i) the metal-free carbon support, (ii) the as-pyrolized carbon composite catalyst, (iii) the as-leached carbon composite catalyst, and (iii) the conventional Pt/C catalyst (20 wt% Pt, E-TEK). The as-pyrolized carbon composite catalyst produced a relatively large amount of H_2O_2, due probably to excess transition metals on the carbon support as discussed in the following section. Upon the subsequent removal of excess metal elements, the H_2O_2 amount decreased to a level less than 2%. Notice that the Pt catalyst generated 1–2% H_2O_2. To our knowledge, such a high selectivity has not been reported for any of transition metal-based or carbon-based catalysts.

Fig. 3 presents the polarization curves of PEM fuel cells prepared with the different cathode catalysts: (i) the metal-free carbon support, (ii) the as-pyrolized carbon composite catalyst, and (iii) the as-leached carbon composite catalyst. The cathode catalyst loadings were maintained at 6.0 mg cm^{-2}. The experiments were performed using 30 psi (2.0 atm) back pressure on both anode and

Table 2
H_2O_2 percentages determined at different disk potentials for the metal-free carbon support, the as-pyrolized carbon composite catalyst, the as-leached carbon composite catalyst, and the conventional Pt/C catalyst (20 wt% Pt, E-TEK)

Disk potential (V, (NHE))	% H_2O_2			
	Metal-free carbon support	As-pyrolized carbon composite	As-leached carbon composite	Pt/C
0.6	0	9.3	1.1	0.4
0.5	1.2	7.1	0.9	0.4
0.4	4.0	6.1	0.7	0.7

cathode compartments. Ohmic potential drop was not compensated for in the measurement. As expected from the RRDE results (Fig. 2), the fuel cell performance increased gradually after the pyrolysis and the chemical leaching. Particularly, it should be noted that the subsequent dissolution of Co and Fe metals from the as-pyrolized catalyst does not cause any activity loss, but rather increases the activity. The PEM fuel cell with the as-leached carbon composite catalyst showed the current densities of 0.27 A cm^{-2} at 0.6 V and 2.3 A cm^{-2} at 0.2 V.

The carbon composite catalysts were synthesized by the deposition of the metal-nitrogen complexes with different compositions (i.e., FeN_x, CoN_x, $Co_1Fe_3N_x$, $Co_3Fe_1N_x$, and $Co_1Fe_1N_x$), followed by the pyrolysis and the chemical leaching. The fuel cell test results are summarized in Fig. 4(a). As shown in Fig. 4(a), the use of Co–Fe–N complex resulted in an improved activity when compared with Co–N and Fe–N complexes, and the maximum performance was achieved for $Co_1Fe_1N_x$. The fuel cell performances of the optimized carbon composite catalyst were presented in Fig. 4(b) for various cathode loadings of 2.0–6.0 mg cm^{-2}.

The electrochemical characterization studies show that the new method involving the $Co_1Fe_1N_x$ deposition followed by the pyrolysis and the chemical leaching produces the carbon composite catalyst with superior catalytic activity (onset potential for oxygen reduction) and selectivity ($\%H_2O_2$) to any of non-precious metal catalysts or carbon-based catalysts reported in the literature [7–27,39–41].

3.3. *Characterizations of metal–nitrogen complexes and metallic species in the carbon composite catalyst*

Fig. 5 demonstrates the k^1-weighted EXAFS spectra in R space for the carbon composite catalysts pyrolized at various temperatures. The catalyst was prepared by the CoN_x deposition onto the metal-free carbon support, followed by the pyrolysis. No chemical leaching was conducted on the pyrolized catalysts. For comparison, a reference spectrum for a pure cobalt foil is given in Fig. 5. As indicated in Fig. 5, the major two peaks centered at R values of ca. 1.2 and 2.1 Å correspond to the Co–N and Co–Co interactions, respectively.

The EXAFS spectrum for the un-pyrolized catalyst shows only a dominant Co–N peak, which confirms the presence of the Co species coordinated with nitrogen groups on the carbon surface. The Co–Co peak becomes strong with increasing the pyrolysis temperature, and only a Co–Co peak is observed when the catalyst was pyrolized at 800 and 1000 °C. This means that the CoN_x chelate complexes decompose at high pyrolysis temperatures above 800 °C, resulting in the formation of the metallic Co species. The EXAFS analysis supports the experimental finding of Yeager [29] that after the heat-treatment of Co-TMPP and Fe-TMPP at 800 °C, neither Co nor Fe was detected in the Mössbauer spectra in a form corresponding to coordination with nitrogen. Therefore, it is clear that the metal–nitrogen complexes are not responsible for the observed activity for oxygen reduction in Figs. 2–4. As a matter of fact, the dissolution of metallic species from the as-pyrolized catalyst increases the activity as presented in Fig. 3.

Fig. 6(a) and (b) presents the TEM images of the metal-free support and the carbon composite catalyst, respectively. The carbon composite catalyst was prepared as follows: (i) the $Co_1Fe_1N_x$ deposition on the metal-free carbon support, (ii) the pyrolysis at 900 °C, and (iii) the chemical leaching in 0.5 M H_2SO_4 solution at 90 °C. Comparing the two TEM images, it is seen that a metal particle was covered with graphitic layers of the carbon composite catalyst, and a nanostructured tube or fiber of graphitic carbon was formed as a result of the pyrolysis in the presence of Co and Fe metals [40,47]. Fig. 7 compares the powder XRD patterns for the metal-free support

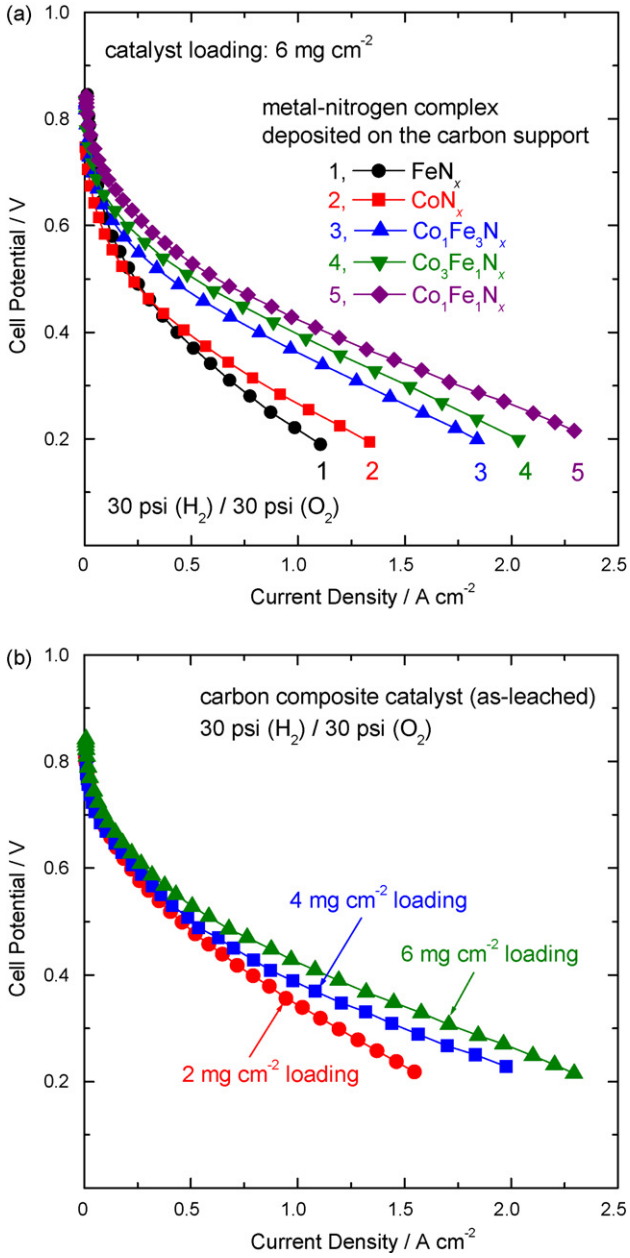

Fig. 4. (a) Polarization curves of PEM fuel cells prepared with the carbon composite catalysts. The catalysts were prepared using the metal–nitrogen complexes with different compositions. All the catalysts were subjected to the chemical leaching. The cathode catalyst loading was 6.0 mg cm^{-2}. (b) PEM fuel cell performances for different loadings of the optimized carbon composite catalyst. The experiments were performed using 30 psi back pressure on both anode (H_2) and cathode (O_2) compartments.

and the carbon composite catalyst. The XRD pattern for the carbon composite catalyst shows the characteristic diffraction peaks that can be assigned to a mixture of the metallic phases (i.e., Co, Fe and Co_xFe_y) and to the cementite phase (Fe_3C).

Table 3 summarizes the concentrations of Co and Fe in the carbon composite catalyst obtained after the chemical leaching in H_2SO_4 solution. The concentrations were determined by ICP-MS and XPS techniques. ICP-MS analysis shows that the concentrations of Co and Fe decreased from 10.4 to 4.6 wt% and from 9.6 to 1.4 wt%, respectively, upon the chemical leaching. XPS detected no metal traces from the leached carbon composite catalyst. Since the escape depth of photoelectrons is a few nanometers, XPS anal-

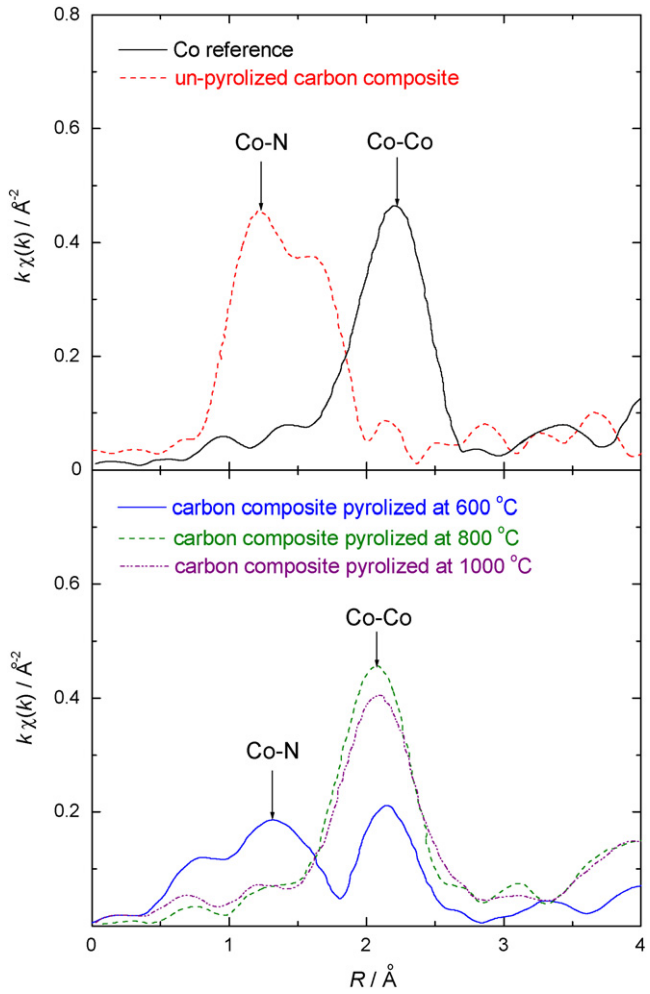

Fig. 5. k^1-weighted EXAFS data for the carbon composite catalysts pyrolized at various temperatures. The catalyst was prepared by the CoN_x deposition onto the metal-free carbon support, followed by the pyrolysis. No chemical leaching was conducted on the pyrolized catalysts.

ysis provides only the surface composition of the carbon composite catalyst. Therefore, the composition analysis by two techniques indicates that Co and Fe particles on the pyrolized catalyst surface were removed by the subsequent chemical treatment in H_2SO_4 solution, whereas metal particles encased in the carbon structure survived the leaching treatment as indicated in Figs. 6(b) and 7.

In summary, the materials characterization studies indicate that (i) the metal–nitrogen chelate complexes are not stable at high temperatures above 800 °C, (ii) no metallic species is present on the catalyst surface after chemical post-treatment, and (iii) the carbon surface is responsible for the observed activity for oxygen reduction.

Table 3
Concentrations of Co and Fe in the carbon composite catalyst obtained before and after the chemical leaching in 0.5 M H_2SO_4 solution at 90 °C, determined by ICP-MS and XPS

Analytical technique		Concentration (wt%)	
		Co	Fe
ICP-MS	(before leaching)	10.4	9.6
	(after leaching)	4.6	1.4
XPS	(after leaching)	0	0

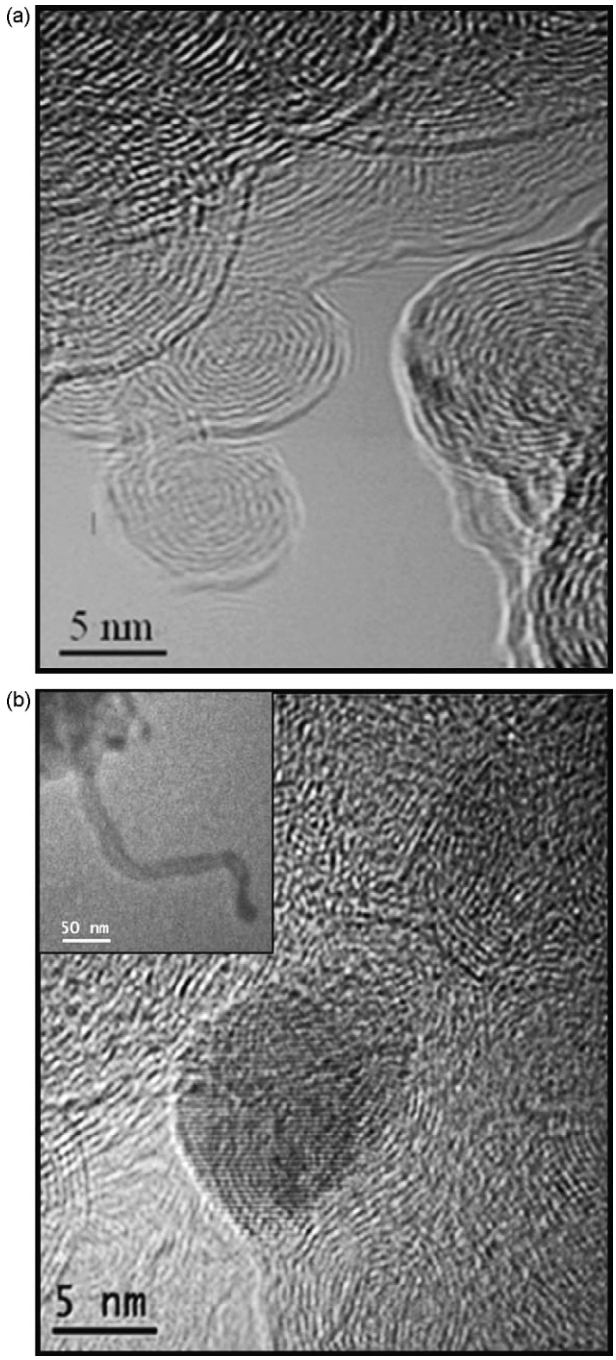

Fig. 6. TEM images of (a) the metal-free carbon support and (b) the carbon composite catalyst. The carbon composite catalyst was subjected to the chemical leaching.

3.4. Characterizations of nitrogen functional groups on the carbon composite catalysts

The nature of nitrogen functional groups was identified using XPS at each synthesis step: (a) after the deposition of $Co_1Fe_1N_x$ complex onto the support, (b) after the pyrolysis at 900 °C, and (c) after the chemical leaching in 0.5 M H_2SO_4 solution at 90 °C. The results are summarized in Table 4 along with the nitrogen content and the fuel cell performance of each sample. The current density and the amount of H_2O_2 were determined at 0.4 V in a fuel cell (Fig. 3) and an RRDE (Table 2), respectively. The activity was determined to be almost zero for the non-pyrolized catalyst, but

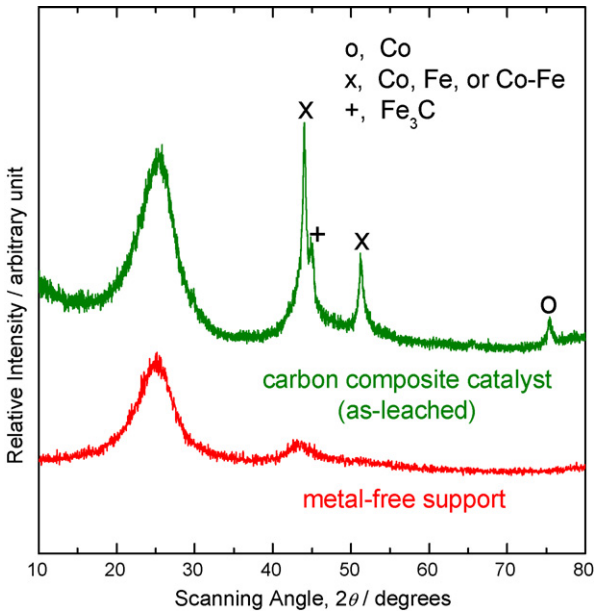

Fig. 7. Powder XRD patterns of the metal-free carbon support and the carbon composite catalyst. The carbon composite catalyst was subjected to the chemical leaching.

the activity and selectivity gradually increased after the pyrolysis and the chemical post-treatment.

The XPS spectrum obtained after the $Co_1Fe_1N_x$ deposition exhibits a broad peak around 398.9 eV that corresponds to the nitrogen groups of the ternary amine-type [48]. The data indicate that the high-temperature pyrolysis induces a significant loss of nitrogen from 9.9 to 2.6 wt%. Upon pyrolysis, the peak splits into three broad peaks at ca. 398.5, 400.5 and 401.1 eV that can be assigned to "pyridinic" nitrogen, "pyrrolic" nitrogen, and "graphitic" nitrogen, respectively. Finally, the XPS spectrum obtained after the chemical leaching shows no dominant peak for pyrrolic nitrogen.

Pyridinic nitrogen refers to the nitrogen atom bonded to two carbon atoms on the edge of graphite planes that is capable of adsorbing molecular oxygen and its intermediates in the oxygen reduction reaction. It has one lone pair of electrons in addition to the one electron donated to the conjugated π bond system, imparting a Lewis basicity to the carbon [47]. Graphitic nitrogen, which is sometimes termed "quaternary" nitrogen, represents the nitrogen atom bonded to three carbon atoms within a graphite (basal) plane.

Recently, Sidik et al. [31] performed the quantum mechanical calculations for oxygen reduction on cluster models of graphite sheets containing substitutional nitrogen (i.e., graphitic nitrogen), and they showed that in acidic media, oxygen reduction is activated to some extent by radical carbon sites formed adjacent to graphitic nitrogen atoms in the basal plane. Using a semi-empirical quantum chemical simulation, Strelko et al. [49] have shown that the highly occupied molecular orbital level (E_{HOMO}) of carbon has a maximum for a nitrogen doping level of ca. 3% providing the high electron-donor ability to carbons. Also, two mechanisms of oxygen chemisorptions on evacuated carbons were suggested: namely, hemolytic (free radical) of a small degree of filling of the surface by oxygen, and heterolytic (large degree of filling) causing the fixation of oxygen on a surface in the form of a superoxide ion O_2^{*-}.

According to Maldonado and Stevenson [47], on nitrogen doped carbon nanofiber electrodes, the oxygen reduction reaction can be treated as a catalytic regenerative process where the intermediate hydroperoxide (HO^{2-}) is chemically decomposed to regenerate oxygen. They have supported the proposed mechanism by electrochemical simulation and by measured difference in hydroperoxide

Table 4
Catalytic activity, selectivity, surface nitrogen concentration, and XPS spectrum at each synthesis step of the carbon composite catalyst

Step	Current Density (A cm^{-2})	% H_2O_2	N content (wt%)	XPS
After metal-nitrogen complex deposition	~ 0	-	9.9	
After pyrolysis	0.7	6.1	2.6	
After chemical post-treatment	1.2	0.7	3.9	

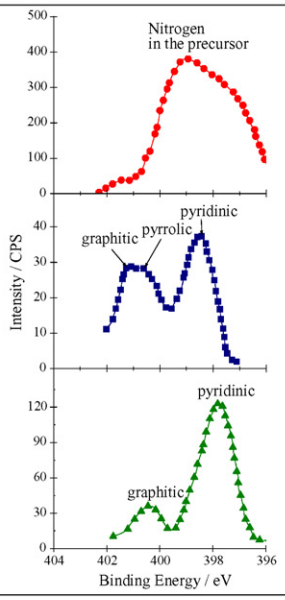

The current density and the amount of H_2O_2 were determined at 0.4 V in a fuel cell (6.0 mg cm^{-2} cathode catalyst loading, 30 psi back pressure) and an RRDE, respectively.

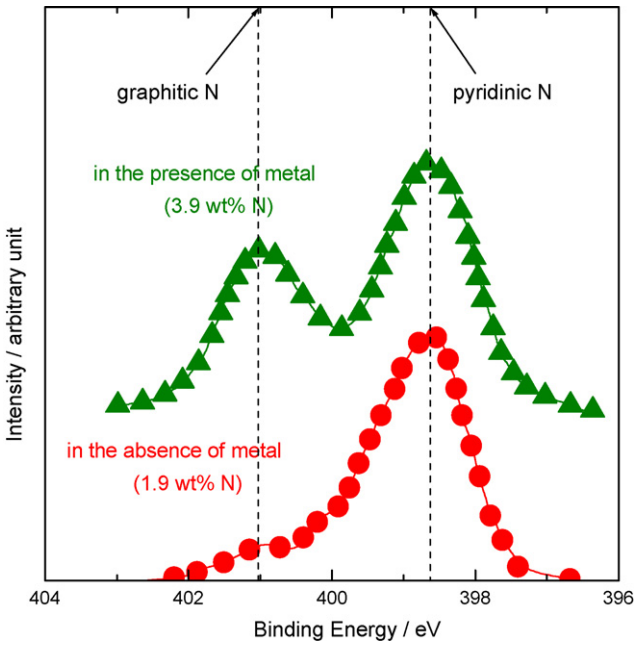

Fig. 8. XPS spectra of N 1s region obtained for the catalysts pyrolized in the absence and presence of transition metals (Co and Fe). The carbon composite catalysts were subjected to the chemical leaching.

decomposition rate constants. The results indicated a remarkable 100-fold enhancement for hydroperoxide decomposition for nitrogen-doped carbon nanofibers. The authors have concluded that pyridinic nitrogen doping into edge plane defects is an important factor for influencing adsorption of reactive intermediates and for enhancing electrocatalysis for oxygen reduction at nanostructured carbon electrodes.

Consequently, the previous simulation analyses and our experimental studies indicate that a strong Lewis basicity of carbons doped with pyridinic and graphitic nitrogens facilitates the reductive adsorption reaction of O_2 without the irreversible formation of oxygen functionalities, due to an increased electron-donor property of carbon.

In order to further study the role of transition metals in facilitating the incorporation of nitrogen functional groups during the pyrolysis, the catalyst was prepared without using any transition metals as follows: ethylene diamine was adsorbed on the metal-free carbon support, followed by the pyrolysis at 900 °C and the chemical leaching in 0.5 M H_2SO_4 solution at 90 °C. The XPS data are presented in Fig. 8. It was found (data not shown) that the catalyst prepared without metal–nitrogen complexes showed no improvement in the activity in comparison to the metal-free carbon support. As indicated in Fig. 8, the surface nitrogen concentration increased from 1.9 to 3.9 wt%, when the pyrolysis was performed in the presence of transition metals.

Yeager [29] and Wiesener [30] have suggested that the transition metals do not act as an active reaction site for oxygen reduction, but rather serve primarily to facilitate the stable incorporation of nitrogen into the graphitic carbon during high-temperature pyrolysis of metal–nitrogen complexes. This means that high-temperature pyrolysis in the presence of transition metals yields a carbonaceous layer with substantial nitrogen groups that are catalytically active for oxygen reduction. Our electrochemical and XPS results also indicate that the high-temperature pyrolysis combined with the chemical leaching facilitates the joint incorporation of pyridinic and graphitic nitrogen groups with a strong Lewis basicity,

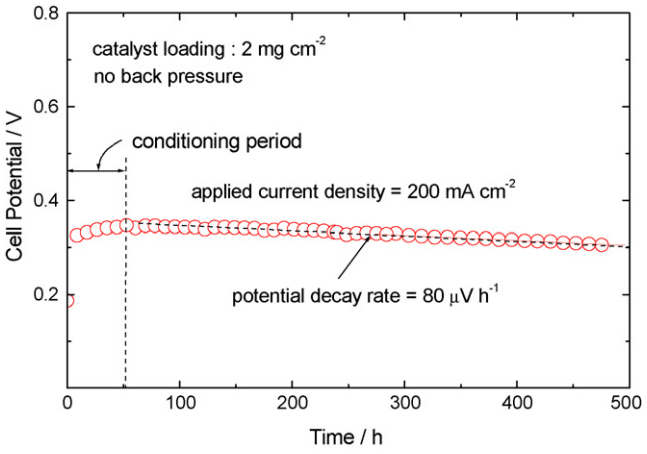

Fig. 9. Galvanostatic potential transient measured on the carbon composite catalyst for stability test. The cathode catalyst loading was 2.0 mg cm^{-2}. The tests were run at 200 mA cm^{-2} using H_2 and O_2 without applying the back pressure.

thus resulting in a high activity and selectivity of carbon composite catalyst.

3.5. Durability study of PEM fuel cell with the carbon composite cathode catalyst

Fig. 9 demonstrates the cell voltage transient measured for the fuel cell with the carbon composite cathode catalyst for stability test. The tests were run at 200 mA cm^{-2} using H_2 and O_2 without applying the back pressure. The cathode catalyst loading was 2.0 mg cm^{-2}. The test result showed an initial increase of potential to ca. 0.35 V, followed by a very slight decay with time (the decay rate ≈80 μV h^{-1}). Note that only ca. 10% performance decrease was observed for 480 h of continuous operation. Fig. 10 compares the XPS spectra of N 1s region for the catalysts taken from the fresh MEA and the MEA tested for 480 h. Two dominant peaks are observed at 398.5 and 401.0 eV that can be assigned to pyridinic nitrogen and graphitic nitrogen, respectively, for both samples. This result con-

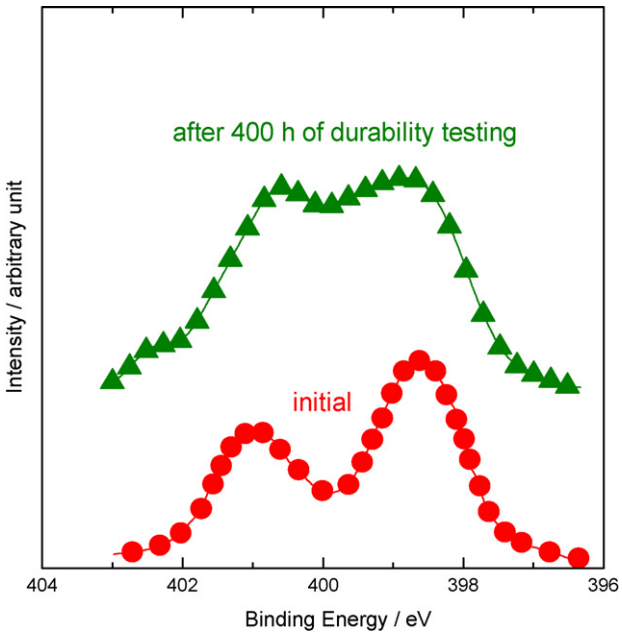

Fig. 10. XPS spectra of N 1s region for the catalysts taken from the fresh MEA and the MEA tested for 480 h.

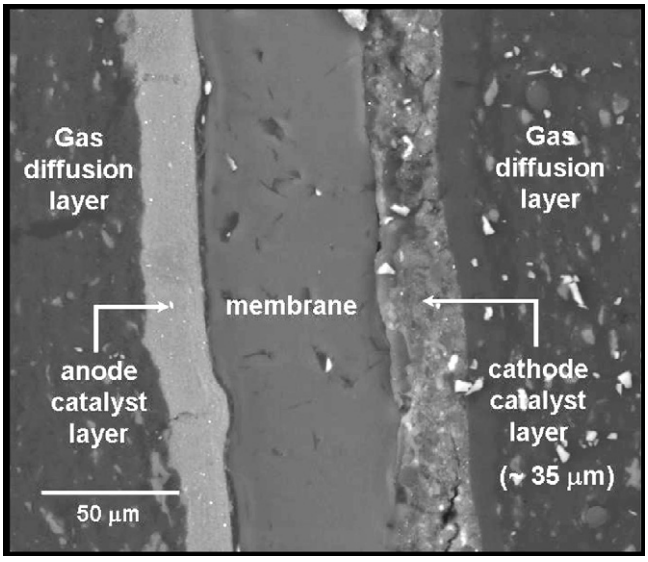

Fig. 11. SEM image of the cross-section of the MEA prepared using the carbon composite cathode catalyst.

firms that catalytically active nitrogen functional groups remain stable on the carbon matrix during long-term fuel cell operation.

Fig. 11 presents a typical SEM image of the MEA prepared using the carbon composite cathode catalyst. The cathode catalyst loading was 6.0 mg cm^{-2}. The image shows the five distinctive layers: (i) anode GDL, (ii) anode Pt/C catalyst layer, (iii) electrolyte membrane, (iv) cathode carbon composite catalyst layer, and (v) cathode GDL. The thickness of the cathode catalyst layer was ca. 35 μm which is thicker than the conventional Pt/C catalyst layer. We found (data not shown) that the fuel cell performance was fully recovered after purging the MEA with O_2, which indicates that an ineffective water management due to a thicker cathode catalyst layer is mainly responsible for a slight performance loss observed in Fig. 9.

4. Conclusions

The new method was developed to synthesize highly active and stable carbon composite catalysts through the high-temperature pyrolysis of Co–Fe–N chelate complex on the support, followed by the chemical leaching. The carbon-based metal-free catalyst developed by us was used as the support. The carbon composite catalyst showed an onset potential for oxygen reduction as high as 0.87 V (NHE) in H_2SO_4 solution, and generated less than 1% H_2O_2. The PEM fuel cell exhibited a current density as high as 0.27 A cm^{-2} at 0.6 V and 2.3 A cm^{-2} at 0.2 V for a catalyst loading of 6.0 mg cm^{-2}. No significant performance decrease was observed for 480 h of continuous fuel cell operation. The EXAFS study showed that the metal–nitrogen chelate decompose at high pyrolysis temperatures above 800 °C, resulting in the formation of the metallic species. All metal particles on the surface were removed by the chemical treatment in H_2SO_4 solution. The XPS results indicated that during the pyrolysis, the transition metals facilitate the joint incorporation of pyridinic and graphitic nitrogen groups into the carbon matrix, and the carbon surface with nitrogen groups is catalytically active for oxygen reduction.

Acknowledgement

The financial support of the Department of Energy (contract no. DE-FC36-03GO13108) is acknowledged gratefully.

References

[1] M.L. Rao, B.A. Damjanovic, J. O'M Bockris, J. Chem. Phys. 67 (1963) 2508.
[2] R.R. Adzic, in: J. Lipkowski, P. Ross (Eds.), Electrocatalysis, VCH Publishers, New York, 1998, pp. 197–242.
[3] N.M. Markovic, P.N. Ross, Electrochim. Acta 45 (2000) 4101.
[4] N.M. Markovic, P.N. Ross, Surf. Sci. Rep. 286 (2002) 1.
[5] H.A. Gasteiger, S.S. Kocha, B. Sompalli, F.T. Wagner, Appl. Catal. B 56 (2005) 9.
[6] R. Jasinski, Nature 201 (1964) 1212.
[7] A. Widelov, R. Larsson, Electrochim. Acta 37 (1992) 187.
[8] G. Lalander, R. Cote, D. Guay, J.P. Dodelet, L.T. Weng, P. Bertrand, Electrochim. Acta 42 (1997) 1379.
[9] R. Cote, G. Lalande, D. Guay, J.P. Dodelet, J. Electrochem. Soc. 145 (1998) 2411.
[10] P. Gouerec, M. Savy, J. Riga, Electrochim. Acta 43 (1998) 743.
[11] P. Gouerec, M. Savy, Electrochim. Acta 44 (1999) 2653.
[12] S.Lj. Gojkovic, S. Gupta, R.F. Savinell, Electrochim. Acta 45 (1999) 889.
[13] S.Lj. Gojkovic, S. Gupta, R.F. Savinell, J. Electroanal. Chem. 462 (1999) 63.
[14] M. Lefevre, J.P. Dodelet, P. Bertrand, J. Phys. Chem. B 104 (2000) 11238.
[15] H. Schulenburg, S. Stankov, V. Schunemann, J. Radnik, I. Dorbandt, S. Fiechter, P. Bogdanoff, H. Tributsch, J. Phys. Chem. B 107 (2003) 9034.
[16] S. Marcotte, D. Villers, N. Guillet, L. Roue, J.P. Dodelet, Electrochim. Acta 50 (2004) 179.
[17] K. Sawai, N. Suzuki, J. Electrochem. Soc. 151 (2004) A682.
[18] D. Villers, X. Jacques-Bedard, J.P. Dodelet, J. Electrochem. Soc. 151 (2004) A1507.
[19] K. Sawai, N. Suzuki, J. Electrochem. Soc. 151 (2004) A2132.
[20] S.-I. Yamazaki, Y. Yamada, T. Ioroi, N. Fujiwara, Z. Siroma, K. Yasuda, Y. Miyazaki, J. Electroanal. Chem. 576 (2005) 253.
[21] M. Yuasa, A. Yamaguchi, H. Itsuki, K. Tanaka, M. Yamamoto, K. Oyaizu, Chem. Mater. 17 (2005) 4278.
[22] F. Jaouen, F. Charreteur, J.P. Dodelet, J. Electrochem. Soc. 153 (2006) A689.
[23] R. Bashyam, P. Zelenay, Nature 443 (2006) 63.
[24] R. Yang, A. Bonakdarpour, E.B. Easton, J.R. Dahn, ECS Trans. 3 (2006) 221.
[25] E.B. Easton, A. Bonakdarpour, R. Yang, D.A. Stevens, D.G. O'Neill, G. Vernstrom, D.P. O'Brien, A.K. Schmoeckel, T.E. Wood, R.T. Atanasoski, J.R. Dahn, ECS Trans. 3 (2006) 241.
[26] J.-H. Kim, A. Ishihara, S. Mitsushima, N. Kamiya, K.-I. Ota, ECS Trans. 3 (2006) 255.
[27] T. Otsubo, S. Takase, Y. Shimizu, ECS Trans. 3 (2006) 263.
[28] F. Beck, J. Appl. Electrochem. 7 (1977) 239.
[29] E. Yeager, Electrochim. Acta 29 (1984) 1527.
[30] K. Wiesener, Electrochim. Acta 31 (1986) 1073.
[31] R.A. Sidik, A.B. Anderson, N.P. Subramanian, S.P. Kumaraguru, B.N. Popov, J. Phys. Chem. B 110 (2005) 1787.
[32] N.P. Subramanian, S.P. Kumaraguru, H.R. Colon-Mercado, H. Kim, B.N. Popov, T. Black, D.A. Chen, J. Power Sources 157 (2006) 56.
[33] Y.-P. Lin, H.-P. Lin, D.-W. Chen, H.-Y. Liu, H. Teng, C.-Y. Tang, Mater. Chem. Phys. 90 (2005) 339.
[34] H.-Y. Liu, K.-P. Wang, H. Teng, Carbon 43 (2005) 559.
[35] P. Kim, H. Kim, J.B. Joo, W. Kim, I.K. Song, J. Yi, J. Power Sources 145 (2005) 139.
[36] P. Kim, J.B. Joo, W. Kim, S.K. Kang, I.K. Song, J. Yi, Carbon 44 (2006) 381.
[37] J.B. Joo, P. Kim, W. Kim, J. Kim, J. Yi, Catal. Today 111 (2006) 171.
[38] V. Raghuveer, A. Manthiram, Electrochem. Solid-State Lett. 7 (2004) A336.
[39] P.H. Matter, U.S. Ozkan, Catal. Lett. 109 (2006) 115.
[40] P.H. Matter, L. Zhang, U.S. Ozkan, J. Catal. 239 (2006) 83.
[41] P.H. Matter, E. Wang, J.-M.M. Millet, U.S. Ozkan, J. Phys. Chem. C 111 (2007) 1444.
[42] B.N. Popov, DOE Hydrogen Program Annual Progress Report, V.C.2, 1–5, 2006.
[43] V. Nallathambi, G. Wu, N.P. Subramanian, S.P. Kumaraguru, J.-W. Lee, B.N. Popov, ECS Trans. 11 (2007) 241.
[44] V. Nallathambi, N.P. Subramanian, G. Wu, J.-W. Lee, B.N. Popov, J. Electrochem. Soc., submitted for publication.
[45] S. Gupta, D. Tryk, S.K. Zecevic, W. Aldred, D. Guo, R.F. Savinell, J. Appl. Electrochem. 28 (1998) 673.
[46] U.A. Paulus, T.J. Schmidt, H.A. Gasteiger, R.J. Behm, J. Electroanal. Chem. 495 (2001) 134.
[47] S. Maldonado, K.J. Stevenson, J. Phys. Chem. B 109 (2005) 4707.
[48] L. Liu, H. Kim, J.-W. Lee, B.N. Popov, J. Electrochem. Soc. 154 (2007) A123.
[49] V.V. Strelko, N.T. Kartel, I.N. Dukhno, V.S. Kuts, R.B. Clarkson, B.M. Odintsov, Surf. Sci. 548 (2004) 281.